Carbon-based terahertz absorbers: Materials, applications, and perspectives

Srisaran Venkatachalam, Klaudia Zeranska-chudek, Mariusz Zdrojek, D. Hourlier

▶ **To cite this version:**

Srisaran Venkatachalam, Klaudia Zeranska-chudek, Mariusz Zdrojek, D. Hourlier. Carbon-based terahertz absorbers: Materials, applications, and perspectives: [Review]. Nano Select, 2020, 1 (5), pp.471-490. 10.1002/nano.202000067 . hal-03043324

HAL Id: hal-03043324
https://hal.science/hal-03043324

Submitted on 7 Dec 2020

HAL is a multi-disciplinary open access archive for the deposit and dissemination of scientific research documents, whether they are published or not. The documents may come from teaching and research institutions in France or abroad, or from public or private research centers.

L'archive ouverte pluridisciplinaire **HAL**, est destinée au dépôt et à la diffusion de documents scientifiques de niveau recherche, publiés ou non, émanant des établissements d'enseignement et de recherche français ou étrangers, des laboratoires publics ou privés.

Received: 10 July 2020 | Revised: 1 September 2020 | Accepted: 8 September 2020

DOI: 10.1002/nano.202000067

nano select Open Access WILEY

REVIEW

Carbon-based terahertz absorbers: Materials, applications, and perspectives

Srisaran Venkatachalam[1] | **Klaudia Zeranska-Chudek**[2] | **Mariusz Zdrojek**[2] | **Djamila Hourlier**[1]

[1] CNRS, Univ. Lille, Centrale Lille, Univ. Polytechnique Hauts-de-France, Institut d'électronique de microélectronique et de nanotechnologie (IEMN) CNRS UMR 8520, Avenue Henri Poincaré, Villeneuve d'Ascq 59 652, France

[2] Faculty of Physics, Warsaw University of Technology, Koszykowa 75, Warsaw, Poland

Correspondence
Djamila Hourlier, CNRS, Univ. Lille, Centrale Lille, Univ. Polytechnique Hauts-de-France, IEMN UMR8520, Av. Henri Poincare, Villeneuve d'Ascq 59650, France.
Email: djamila.hourlier@univ-lille.fr

Correction added on October 7, 2020 after first online publication: The surname for author Klaudia Chudek has been corrected.

Abstract

Terahertz (THz) waves are nowadays used in a multitude of applications ranging from medicine, telecommunication, security surveillance, to fast sensing and imaging. Along with the most apparent aspects of the potential applications, there is also a flip side of the coin: the effects of unwanted electromagnetic pollution on various elements of the environment. Therefore, an effective shielding of THz radiation, preferably with an appreciable amount of absorption, is one of the milestones for the further development of terahertz technology. This review briefly outlines the main aspects of the area of research in terahertz absorbers, materials used, and their specific applications. Particular attention has been paid to the use of carbon-based materials as terahertz absorbers, needed to fill the gap between the well-known components across absorption coefficient 10–100 cm^{-1} for a refractive index 3–5. An example of such a class of materials is that of the organic or hybrid organic–inorganic polymers whose pyrolysis in an inert atmosphere gives black materials containing a residual free carbon phase. The carbon phase is a random network of covalent bonds in which carbon atoms are mainly in sp^2 hybridization state. The absorption of THz radiation is strongly dependent on the state of arrangement of C-sp^2, the amount of carbon, and the graphitic carbon domain size.

KEYWORDS
absorbers, carbon, composites, submillimeter waves, terahertz

1 | INTRODUCTION TO TERAHERTZ DOMAIN

Terahertz (THz) waves are the electromagnetic (EM) waves covering the frequency gap that lies between microwaves and infrared radiations (Figure 1). The THz domain corresponds to frequencies of 0.3 THz–10 THz, which is equivalent to the wavelengths from 1 mm to 30 μm.[1] This EM range is also known as T-rays, THz gap, sub-millimeter waves, or far-infrared radiations.[2]

Terahertz technology nowadays has a wide range of applications, Table 1 lists some applications in different field of terahertz radiation.

Exploitation of THz technology allows certain benefits when compared to conventional techniques. For example, in the diagnosis of cancer, THz imaging is a non-ionizing

This is an open access article under the terms of the Creative Commons Attribution License, which permits use, distribution and reproduction in any medium, provided the original work is properly cited.
© 2020 The Authors. *Nano Select* published by Wiley-VCH GmbH

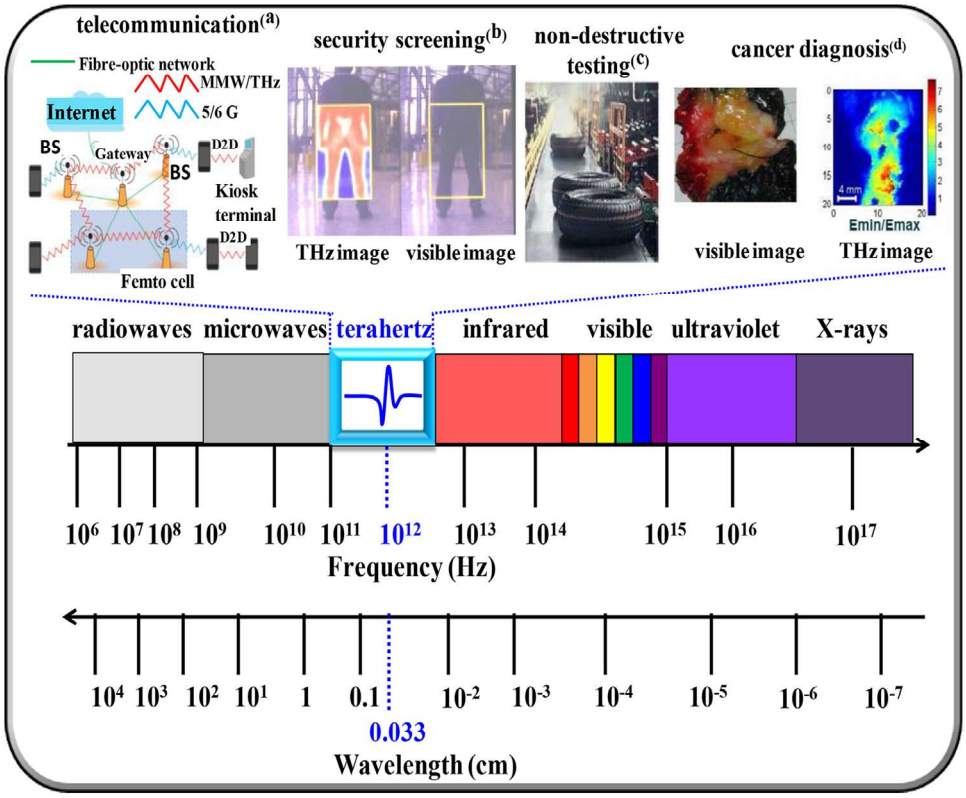

FIGURE 1 The terahertz domain in the electromagnetic spectrum and its applications; a – Nagatsuma et al.,[3] b –Tactical Solutions, NZ,[4] c, d – Terasense Group Inc., UK[5]

TABLE 1 Most common applications of terahertz technologies

Application	THz integrated systems	Purpose
Chemistry	Spectrometer (Time-domain, far-infrared Fourier transform spectrometer)	Identification of large molecules units like polycrystalline glucose (sugar),[6] Lactose,[7] weak intermolecular interactions such as hydrogen and van der Waals bonds,[8]
Medicine	THz imager	Cancer (breast, prostate, skin) diagnosis[9] 3D graphic images of demineralized tooth[7]
Non-destructive testing	THz camera	Identification of metal objects in automobile tyres, metal objects in postal service, non-contact detection of explosives,[5]
Homeland security	THz camera/scanner	Large-area surveillance,[5] Identification of ceramic weapons[10]
	Inteferometers (IRAM, Plateau de Bure, France)	Operates at 230 GHz with a capability of resolving apple at a distance of 30 km[11]
Astronomy	Satellites	Infrared astronomical satellite (IRAS, NASA) – discovery of comet iras-araki-alcock at 12 THz;[6] Cosmic Background Explorer COBE, NASA) detection of infrared radiation of cosmic background, structure of milky way and interstellar dust.[6]
Telecommunications	Antenna-based transmitter and receivers	High-definition data transfer,[12] combined with 5G wireless technology[3]

and non-destructive tool that easily distinguishes cancer cells from their normal counterparts. Due to the different water content in cells, different THz absorptions can be observed. The cell-variations in water content produce the contrast in the THz imaging.[9] In telecommunication systems, the increase in frequency from microwaves to the sub-millimeter domain allows the transmission of uncompressed high-resolution and high-definition wireless data, with transfer rates of 11 Gbit s^{-1} at 0.2 THz[13] and 1.5 Gbit s^{-1} at 0.6 THz with 10 nW signal.[12] In

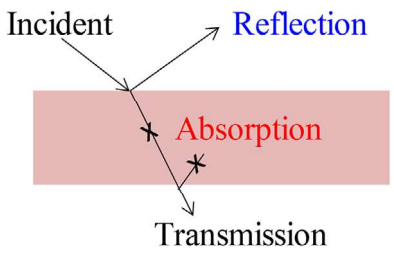

FIGURE 2 The schematic diagram showing the three fundamental wave-material interactions

security systems, the advantages of using THz are also vast, including the possibility of remote detection (up to 30 m) of hidden objects with ultra-high scanning speed (more than 50 times faster than the time for X-ray systems) and at the same time, these radiations are inoffensive and harmless to people.[14] However, some of the problems[2] remain unsolved, such as:

- development of more powerful, stable sources and sensitive detectors
- efficient transport of the THz wave from transmitter to receiver
- acquisition of real-time images with a good signal-to-noise ratio and adequate spatial resolution
- standardization and calibration of spectral reference for THz detectors
- development of an efficient absorber suitable for broadband frequencies.

The existing devices, being used in neighboring domains, are either incompatible or inefficient at THz frequencies. For example, thermal detectors that convert incident radiation into heat are not efficient for THz frequencies because most of the wavelengths of the THz radiations are not absorbed.

In this study, particular attention has been given to absorbers, specifically adapted to the THz domain. Such absorbers can be exploited for plenty of purposes in most integrated systems such as filters and attenuators.

1.1 | Terahertz absorption

The incident THz waves on material undergo three main processes: reflection, transmission, and absorption, as shown in the schematic diagram (Figure 2).

Absorption is defined as a process in which the energy of an EM wave is converted to other forms of energy, mostly heat energy. Here and elsewhere in the manuscript, the measured quantities are represented by the terms: absorbance (A), transmittance (T) and reflectance (R), and multiple internal reflections (MIR). Absorbance is given by the relation (1) as,

$$A = 1 - T - R - \text{MIR} \tag{1}$$

where T is defined as the ratio of transmitted power (P_t) to the incident power (P_i). Likewise, R and A are the power ratios of reflected and absorbed radiations, respectively. The power ratio is expressed either in linear scale or in decibel (dB) scale. The formula for converting from linear scale to dB scale can be expressed as Equation (2), which is also often called shielding efficiency (SE) in the EMI shielding community. The 10 dB of T (or SE) means that 1% of initial radiation passed through the material and 99% has been blocked (20 dB—99.9%, 30 dB—99.99%, etc.)

$$T\ (\text{dB}) = 10 \times \log_{10}\left(\frac{P_t}{P_i}\right) = -\text{SE}\,(\text{dB}) \tag{2}$$

The penetrating wave can be reflected internally by any boundaries inside the material causing an important contribution (MIR) to the wave attenuation. MIR is particularly important for porous materials with porous structure (e.g., composites foams) or in case of certain geometrical architectures (e.g., Meta materials). However, for good THz absorbers (SE > 10 dB) MIR process can be fully neglected[15] and A or absorption component of the SE can be expressed as:

$$A\,(\text{dB}) = 10 \times \log_{10}\,(T/(1-R)) = -\text{SE}_\text{A} \tag{3}$$

The magnitude of T, R, A depends on the frequency of EM waves, and on the nature of the material itself. For example, the THz spectrum of CNT-based organic coating (chemical composition of the matrix is not available in Ref.[16]) of thickness 80 μm on transparent substrate is shown in Figure 3.The absorbance is nearly 100% at frequencies ≥ 2.5 THz (wavelengths of ≤ 100 μm) and decreases to 50% at frequencies ≤ 0.6 THz (wavelengths of ≥ 500 μm). At higher wavelengths, the THz wave can penetrate through the coating and is reflected from the back. For that reason, the reflectance increased up to 40% at 0.6 THz. Such spectral responses are not suitable for broadband absorbers, particularly for terahertz thermal detectors.[16] Absorption can be enhanced by increasing the thickness of the coating but to the expense of the detector response which becomes slower.

For perfectly absorbing materials, two requirements must be satisfied in order to prevent:

- wave reflected ($R \to 0$): the impedance (effective resistance) of the material surface must be identical to the free-space impedance (377 Ω)

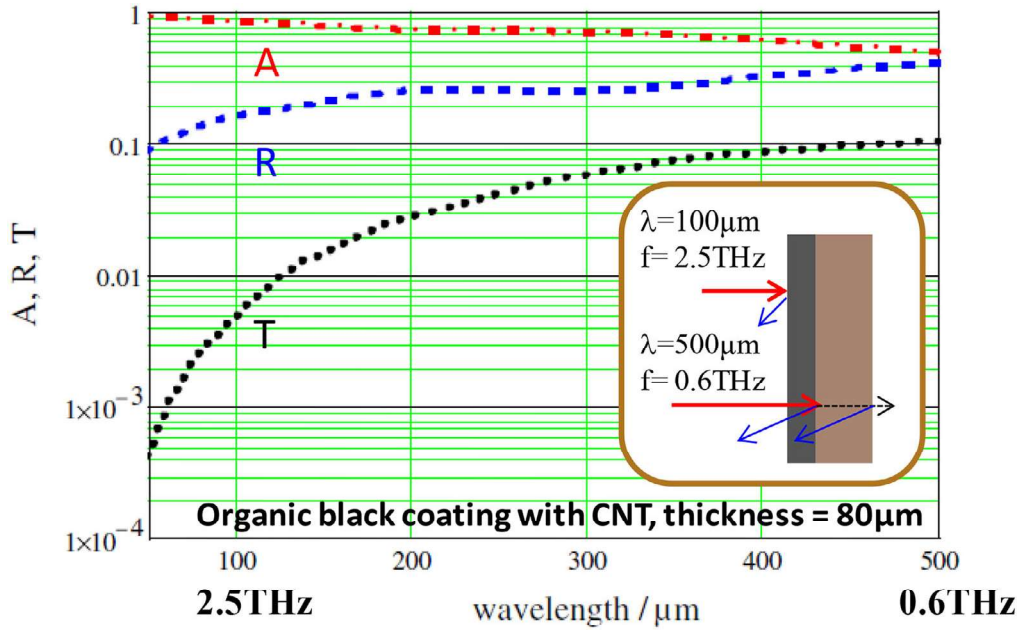

FIGURE 3 Transmittance (T), reflectance (R) and absorbance (A) of carbon nanotubes –based organic black coating of thickness 80 μm on transparent substrates. Adapted with permission from Ref.[16]

- wave transmitted ($T \rightarrow 0$): a material with a high absorption coefficient α is required over the entire terahertz band.

In addition to the three fundamental processes, there are also many other interactions between the THz wave and the material, such as refraction, scattering, diffraction and interferences. These phenomena depend not only on the material properties (as surface state, thickness, optical constants), but also on the incident THz wave characteristics (angle of incidence, wavelength, polarization).

The refractive index n (unit less) of a material is defined as the ratio of velocity of light in free space (in air) *to* its velocity in the material. The velocity of light in free space is $c = 3 \times 10^8$ ms^{-1}. The absorption coefficient α determines how far the THz wave can penetrate into a material before it gets absorbed. The unit of α is cm^{-1}. n and α are intrinsic parameters of material known as optical constants, that is used to quantify the interaction of THz wave with the material. These parameters strongly depend on the frequency of the incident radiation.

1.2 | The THz absorption behavior of common materials

1.2.1 | Electrical insulators

Electrically insulating materials can be classified into two types depending on their chemical composition: organic-polymers and ceramics (oxides: SiO_2, Al_2O_3 etc., or nitrides—Si_3N_4, AlN, etc.). The polymers have the smallest refractive index (1.3–1.5), leading to less reflection loss (~ 3–4% at normal incidence) and quite low absorption coefficient (< 0.28 cm^{-1}). The reflection loss at normal incidence can be calculated using the relation (4),

$$R = \left[\frac{n-1}{n+1}\right]^2 \tag{4}$$

For organic polymers, the reflection loss is very low, around ~3–4%. However, a strong absorption occurs at characteristic frequencies ascribed to the resonance of the incident wave with the molecular vibration of the polymers. From THz absorption measurements using a THz time-domain spectrometer, Cunningham *et al.*[17] deduced the optical constants of many commercially available polymers such as polyimide (PI, Kapton), polymethylmethacrylate (PMMA), polystyrene (PS), polyethylene cyclic olefin copolymer (Topas), polytetrafluoroethylene (PTFE, Teflon®) over a broadband. The authors observed that the resonance absorption occurs in Teflon at 6.1, 8.3 THz, in Kapton at 4.9, 6.1 and 7.8 THz, and in PMMA at 2.7 and 6.6 THz. Due to the resonance absorption, such materials cannot be used for broadband THz applications as passive components like lenses, beam splitters, optical windows, or substrates. The suitable materials are Topaz $Al_2SiO_4(F,OH)_2$ ($n \sim 1.524$, $\alpha < 2.9$ cm^{-1}) and PS ($n \sim 1.59$, $\alpha < 3$ cm^{-1}) due to relatively invariable optical constants across the entire THz regime. Oxides such as SiO_2 (fused,

and quartz) have a slightly higher refractive index than organic polymers, but the absorption coefficient depends on the crystallinity. For example, the fused silica has an absorption coefficient of < 8 cm^{-1}, whereas quartz has very small value of < 0.7 cm^{-1}. The major disadvantage of quartz is that it might reflect the radiation due to its birefringence properties. However, Quartz is well suited to optical purposes as window material.[2]

1.2.2 | Semiconductors

Silicon and germanium semiconductors of high-purity are transparent throughout the THz domain. The intentional addition of certain dopants creates shallow donor or acceptor levels in the band gap of the semiconductor. The added dopants generate free carriers in the material. Due to the different concentrations of free carriers in the material, different THz absorptions can be observed. However, the high refractive index of Si ($n \sim 3.42$, at 1–10 THz) and Ge ($n \sim 4$, at 1–10 THz) leads to reflection losses greater than 30% at normal incidence.

1.2.3 | Metals

Metals have a very high refractive indices and high absorption coefficients in the THz domain.[18] For instance, gold, $n = 447$ and $\alpha = 2.34 \times 10^5$ cm^{-1} at 1 THz.[18] Metals are an essential part of optical elements, in the form of, for example, mirrors, waveguides, light-pipes, and Winston cones.[2] Metals can be used as absorbers only when the thickness is lower than its skin depth.[19] The skin depth δ, defined as the distance at which the electric field of the penetrated wave falls to 0.366 times of its initial value, related to the electrical conductivity $\sigma_{d.c.}$, relative permeability μ_r of the metal and frequency f of the THz radiation, according to the relationship (5)

$$\text{Skin depth } \delta = \sqrt{\frac{1}{\pi f \sigma_{d.c.} \mu_r}} \tag{5}$$

For gold, the skin depth is 75.3 nm, calculated using bulk electrical conductivity $\sigma_{d.c.} = 4.45 \times 10^5$ S cm^{-1} and $\mu_r = \mu/\mu_o$, where $\mu = 1$ (non-magnetic material), μ_o (permeability of free-space) $= 4\pi \times 10^{-7}$ Henry meter^{-1}. The absorption depends not only on metal thickness, but also on the sheet resistance of the metallic layer. The sheet resistance is related to the electrical conductivity $\sigma_{d.c.}$ and to the thickness L_s of the metallic layer, as $\frac{1}{\sigma_{d.c.} \times L_s}$. In other words, a metal having the highest electrical conductivity requires the lowest thickness of metal. Hadley and Dennison[20] claimed that the maximum of 50% absorbance (Figure 4)

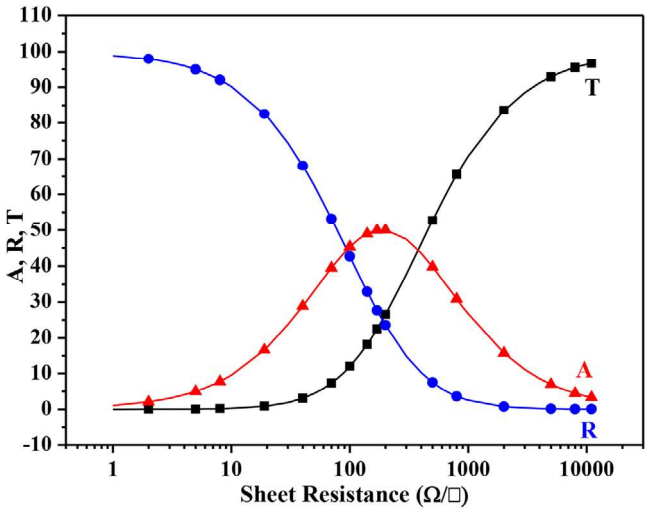

FIGURE 4 Transmittance, reflectance and absorbance of an unsupported metallic film as a function of sheet resistance[20]

can be obtained using a metallic layer with a sheet resistance of 188.5 ohms (Ω) per square (□).

The metallic layers having a high sheet resistance ($> 10^4$ Ω □$^{-1}$) are transparent ($T = 100\%$), whereas those having a low sheet resistance (1 Ω □$^{-1}$) are reflective ($R = 100\%$). Ideally, for maximum absorbance, a gold thickness of 2 nm is required. Gold films of nanometric thicknesses, preferentially uniform, are difficult to achieve. As an alternative solution, the thickness was increased to 50–150 nm with the help of a less electrical conductive material than gold, as for example, Bismuth that has an electrical conductivity of 7.75×10^3 S cm^{-1} at room temperature.

2 | CARBON-BASED MATERIALS

2.1 | General outline and classification

Among the functional materials devoted to THz absorbers, carbon-based materials have received much attention due to their variety of allotropic forms and morphologies, exhibiting different properties.[21] For instance, Carbon-based materials have electrical properties spanning from insulators to conductors depending on their allotropic structure. The sp^2 bonded carbons such as graphite, carbon nanowhiskers, and nanotubes have high absorption coefficients $\alpha_{\text{graphite}} \sim 1.3 \times 10^3$ cm^{-1} and refractive indices $n_{\text{graphite}} \sim 16$ in THz domain. The well-known allotropic forms of carbon are graphite (sp^2 carbon) and diamond (sp^3 carbon). These two materials have complementary properties in the THz frequencies. Graphite is black, opaque (THz), and is a good conductor of electricity, whereas diamond is transparent (THz) and electrical insulator. In graphite, free-carriers are responsible not

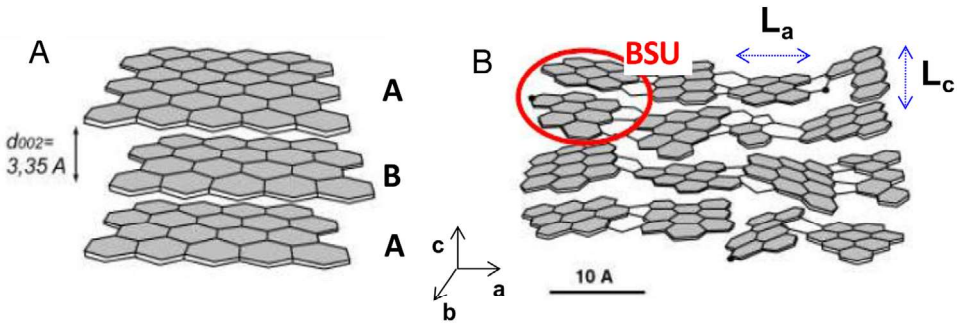

FIGURE 5 Structure of (A) graphite and (B) turbostratic carbon[24,25]

only for strong absorption but also for the high reflection in the THz domain. In the frequency range 0.1–2 THz, the refractive index n varies from 16–4, respectively, while the absorption coefficient α varies between (1–3.2) × 10^3 cm^{-1}.[22] Diamond has an absorption coefficient of 0.05 cm^{-1}, and a refractive index of 2.38 leading to reflection loss of 16.7% at normal incidence.[23] In graphitic materials, the basic repeating structure is a graphene layer, in which the monolayers of carbon atoms are arranged in a hexagonal ring (honeycomb lattice) structure along the "a" axis (Figure 5).

The carbon atoms are strongly linked by covalent bonds, that is, three sp^2 electrons as sigma bonds, and the fourth p electrons as π bonds. This structure is largely responsible for good electrical conductivity and thermal conductivity. In graphite, many graphene layers are stacked in ABAB fashion along the "c" axis that extends to the semi-infinite. The interatomic distance (bond length) between two carbon atoms in a-axis is 0.142 nm, which is shorter than the distance between two layers 0.335 nm.[21] Due to a weak bonding (van der Waals) between the graphene layers, the graphite is soft, thus it is used for lubrication purposes. For THz absorption, however, the bulk graphite is not well suited due to its highly reflective character (Reflectance, R ~ 99%).[26] Reflection can be minimized only if the sheet resistance of graphite approaches the value of 377 Ω (the free-space impedance). However, due to the high electrical conductivity of bulk graphite, it is difficult to reach such a value; this is still a challenging task.

Low-dimensional carbon derivatives offer a plethora of possibilities in terms of atomic/molecular structures, shape, and dimension, either as an additive or as main building block for electromagnetic interference (EMI) shielding applications.

In the subsequent section, we present a brief description of major types of carbon low dimensional-based materials which are tailored to improve EMI shielding in terahertz domain.

2.2 | Carbon-based polymer composites

One of the strategies to modulate absorption of bulk graphite, or any carbon phase, is to mix it with another material called matrix. The resulting mixed phases (filler and matrix) is a composite material. Usually, the matrix is chosen as a THz transparent material that holds the absorbing fillers, and the absorption is controlled by the weight fraction, the geometry, and distribution of the fillers in the matrix. Carbonaceous fillers may be of variable structure and shape, such as graphite particles,[27] carbon nanofibers (CNF),[28] carbon nanotubes (CNT),[29,30] onion-like carbon (OLC),[31] graphene,[32] carbon black,[30] and carbon nanowhiskers.[33]

For example, the addition of 5 wt.% Graphene-oxide filler[34] in a polyethylene matrix enhanced the absorption coefficient from 0.3 to 12 cm^{-1} at 0.5 THz, while the refractive index increased slightly from 1.45 to 1.53.[34]

The materials can be classified as: (i) bulk composites with carbon fillers embedded into organic polymer matrix, (ii) thin films of carbon on dielectric substrates, such as quartz,[32,35] cellulose,[36] polyethylene-terephthalate (PET),[37] fluoroacrylic co-polymer (PMC),[33] and (iii) carbon foams.

Figure 6 shows the effect of carbon-based fillers of composites on shielding effectiveness (SE). Clearly, the SE depends greatly upon the amount of fillers, their shape and their dispersion in the matrix, and probably their hybridization state and allotropic form. For the same concentration of carbon filler (1 wt.%), filamentary shaped carbon structures MWCNT seem to be more efficient absorbers than their spherical counterparts, carbon black (CB) and onion-like carbon (OLC)).

Polley et al.[41] reported on a PVA (polyvinyl acetate) composite with different concentrations (0.1% to 2% by weight) of single-walled carbon nanotube (SWNT) fillers. In the broad terahertz range 0.3–2.1 THz, a linear relation between SWNT loading and SE has been found. In the low frequency range 0.3-0.6 THz, the SE exhibits low

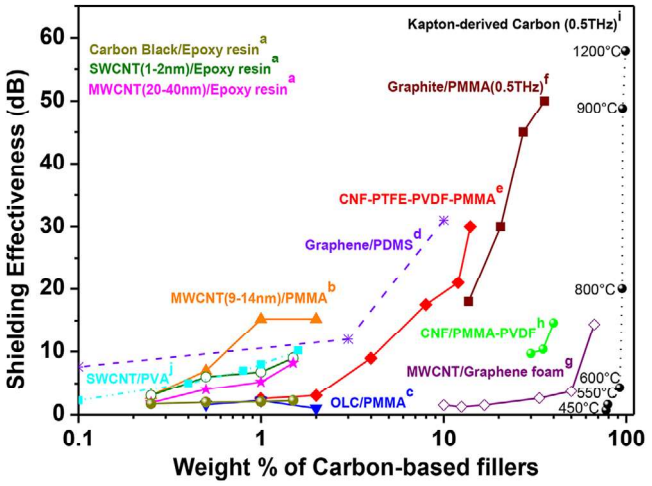

FIGURE 6 Shielding effectiveness of carbon-based composites at 0.5-0.6 THz; a – Macutkevic et al. (2012),[30] b – Macutkevic et al. (2012),[29] c – Macutkevic et al. (2008),[31] d – Zdrojek et al. (2018),[38] e – Das et al. (2011),[28] f – Seo et al. (2008),[27] g – Huang et al.(2018),[39] h – Das et al. (2012),[33] i – Venkatachalam et al.,[40] j – Polley et al[41]

values (10 dB) and the transmittance reaches 60%. However, the transmittance dropped almost to zero for frequencies above 2 THz. Based on the obtained characteristics, the authors suggest that, the SWNT/PVA composites may be better suited for low band pass THz filtering application.

Chamorro-Posada et al.[34] conducted a comparative study on four different carbon fillers (graphite, needle coke, graphene oxide, and reduced graphene oxide) embedded into a PE matrix. The shielding and optical properties were studied in the 0.5 - 3 THz range. Graphite filled PE composite exhibited the highest values of absorption coefficient (~125 cm^{-1}), followed by needle-coke (~39 cm^{-1}), GO (~7 cm^{-1}), and rGO (~15 cm^{-1}), at 2.3 THz for filler concentration of 2.5 wt.%. Such differences in the absorption were attributed to the degree of stacking aromatic carbon layers and the existence of interplanar vibrations.

Recently Zdrojek et al.[38] presented a series of nonconductive PDMS composites containing three different contents of graphene flakes inclusions (0.1, 0.2, and 10 wt.%), fabricated via a simple blend-mixing method. The samples in form of flat disks, approximately 0.8 mm thick were tested within 0.1–0.8 THz using a custom made THz-TDS setup. They claimed that the main shielding mechanism of composite materials was absorption rather than reflection, based on the shielding effectiveness components ratio (SE_{ABS} and SE_R). The sample with the highest graphene loading (10 wt.%) exhibited the highest SE value of 30 dB at 0.6 THz.

At a filler content of 13 wt.%, CNF (average diameter 100 nm)[28] and graphite particles (26 μm diameter)[27] reveal comparable values of SE ~ 20 dB. It is worth mentioning that both CNF and graphite are issued from high temperature treatments > 3000°C.[28] These heated materials are composed of well-organized sp^2 carbon and contain a very low concentration of heteroatoms.

Although the SE increases with the filler content, a maximum amount of graphite can be dispersed in a PMMA matrix is 35.7 wt.% (SE 50 dB for a ~300 μm thick sample). Further addition of the graphite leads to fragile composite materials.[27]

In general, all these composites suffer from inhomogeneity of the dispersed phase and reproducibility/reliability, which are unavoidable in the fabrication of composite materials via mechanical mixing.

2.3 | Carbon thin films

Thin films can be prepared from carbon nanomaterials, with or without a binding agent, and using various fabrication methods including vacuum filtration, ink-jet printing or spin coating.[33,35,37,42,43] Slightly different types of thin films are those that are too fragile and require a substrate to avoid damage during preparation and handling.

Das et al.[28] used cellulosic substrates sprayed with a mixture of PTFE particles and carbon nanofibers into a polymer blend solution of PVDF and PMMA. The SE was measured in a relatively narrow range between 0.56 and 0.63 THz. The authors found that the use of CNF has a beneficial effect on the electrical conductivity. For an optimum ratio of CNF/polymer = 1.1, the SE is directly proportional to the film thickness of 24 to 70 μm. In the studied frequency range, the maximum SE of ~40 dB was obtained for 70 μm thick films.

Polley et al.[44] showed another example of a free-standing carbon film constituted only by MWCNT, of equal lengths, but of different diameters (7, 25, and 40 nm). This study was performed within the frequency range 0.4 - 2.2 THz, and using commercial THz-TDS setup allowing the evaluation of the three characteristics of SE: reflection, absorption, and multiple inner reflections (MIR).

The SE of MWCNT films gradually increased at higher frequencies with a maximum of around 21 dB at 2.2 THz for the film thicknesses in the range of 15 to 22 μm, and containing MWCNT of 25 and 40 nm diameters.

The contribution from MIR is often omitted in most scientific works, in particular, for highly absorbing materials (> 10 dB) in THz domain. Polley and coworkers have provided such information in their publication. They point out that because of the very low thickness of the sample, the THz radiation undergoes multiple back and forth reflections between interior surfaces of the thin film, and therefore an additional factor (SE_{MIR}) should be considered.

They found the SE_{MIR} negative and approaches 0 dB, at 2.2 THz.

Another type of carbon thin film worthy of distinction is a stacked graphene that is made of relatively large sheets of graphene monolayers fabricated using CVD process, and then transferred on top of each other to form graphene multilayers.[32,45]

Baek et al.[46] showed that the transmittance decreases with an increasing number of graphene layers. Stacking of 12 layers of graphene leads to the lowest transmittance of 27%, and thus to a relatively good shielding performance, considering the thickness of the sample of 4.08 nm.

Yan et al.[32] demonstrate that the SE can be increased by stacking alternating graphene layers and thin intermediate layer of nanofilbrillated cellulose (NFC). The SE was improved up to 16 dB for 5-graphene layers.

Dong et al.[47] report on a flexible, free-standing rGO (reduced graphene oxide) paper fabricated via a process involving two steps: chemical reduction using hydroiodic acid followed by a heat treatment in argon at three different temperatures, namely, 400°C, 600°C, and 800°C, for 2 hours. The EMI shielding of films was studied in 0.1–1 THz range using time-domain terahertz spectroscopy (THz-TDS). Results for all rGO samples show similar trends in shielding effectiveness (SE) versus frequency. It was found that the temperature of heat treatment is an important parameter affecting the SE properties of films. For materials heated up to 400°C, the heating process was beneficial as their SE are greater than 60 dB at frequencies beyond 0.4 THz, travelling through ~370 μm thick film.

The 400°C heated material showed the highest SE value when compared to unheated films. Also notice that the heating process led to an increase in the electrical conductivity of the rGO samples. High conductivity often results in strong reflection of THz radiation and relatively lower absorption.

However, too high a treatment temperature can be harmful and depends on the thermal stability of the phases present in the material. For instance, the 400°C film exhibited absorption of 16%, at 0.6 THz, whereas, the heated materials at higher temperatures resulted in a decrease in their total SE and also in their electrical conductivity. This is attributed to removal of carbon from materials during the heating process. XPS and Raman analysis suggested decomposition reaction had occurred between carbon and oxygen present in the material, and led to the loss of carbon in the form of CO and CO_2.

Figure 7 shows shielding effectiveness of carbon-based thin films as a function of film thickness, at the frequency 0.6 THz.

In closing this section, it might be well to mention that the extent of THz absorption by materials is governed by many parameters such as the type of filler, the thickness, and the nature of the matrix. It would be difficult to make any comparison between the materials, as several parameters are not mentioned in the available scientific literature. Nevertheless, it would seem that filamentary forms such as CNTs absorb waves more efficiently than graphene. Moreover, whatever stacking order and number of graphene layers, a configuration made out of only stacks graphene layers seems to be less efficient THz absorber than the 3D graphitic structure.

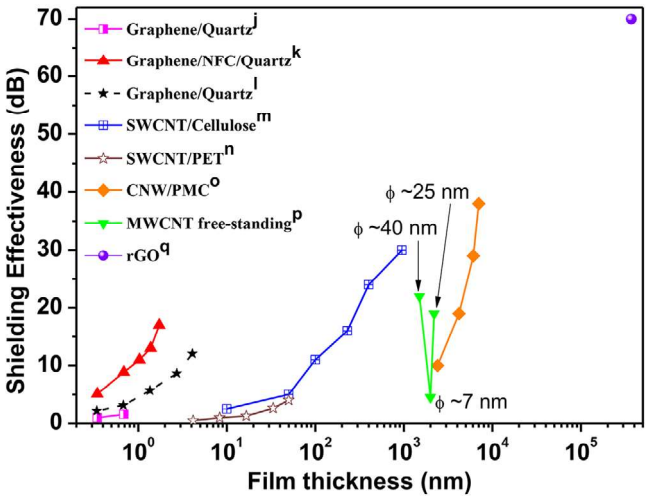

FIGURE 7 Shielding effectiveness of carbon-based thin films and graphene stacks; j – Sensale et al. (2008),[35] k – Yan et al. (2012),[32] l – Baek et al. (2013),[46] m – Jung Taek et al.(2012),[36] n – Seo et al. (2008),[37] o – Das et al.(2012),[33] p – Polley et al.(2016),[44] q – Dong et al.(2018)[47]

2.4 | Carbon-based foams

Carbon based foams are a relatively new group of materials for terahertz absorber applications. The key feature of the carbon based foams is their inner porous structure. The pore network contains void spaces that act as cavities in which the transmitted THz radiation undergoes multiple reflections and eventually gets absorbed by the material. Another attractive advantage of the foam absorber is its low density, thus making it a lightweight material, for stealth applications. Specific shielding effectiveness (SSE) or specific average terahertz absorption performance (SATAP), represented in dB g^{-1} cm^3, are widely used to identify and estimate physical properties of porous materials.[48,49] Because of their inner structure, the foam samples are usually thicker than thin films or bulk composites, but they also can be easily compressed into smaller thicknesses.

There are a number of methods to fabricate foam structures, using template, gas bubbling, carbon-based

foaming agents generating volatile gases by thermal decomposition, etc. For more detailed fabrication methods of carbon foam, the reader is referred to papers and reviews.[50,51]

While the subject of EM wave absorption ability of carbon foam materials has been extensively studied in microwaves range, less has been accomplished in terahertz domain.

Huang et al.[39] showed a study on graphene foam (GF) and multiwalled carbon nanotubes/multiwalled graphene foam (MGF) fabricated by modified solvo-thermal reaction. The samples were prepared in various MWCNT/G ratios and then heat at temperatures ranging from 400°C to 1500°C in argon atmosphere. The heat treatment leads to a noticeable change in the density of samples. The density decreased from 1.7 mg cm^{-3} for unheated materials to 0.83 mg cm^{-3} for those heated at 1500°C. The optical measurements were conducted in 0.1–1.6 THz range using THz-TDS system. The best EMI shielding obtained for GFs and MGFs are 74 and 61 dB, respectively, for 3 mm thick samples. They identified that absorption is the main shielding mechanism in the foams. The SATAP values of porous materials reached ~1.8×10^4 dB cm^3 g^{-1}. The major drawback of these carbon foam materials is their poor mechanical strength. In an effort to improve the THz absorption performance, the same group of researchers[48] has substituted MWCNT by MXenes ($Ti_3C_2T_x$) nanosheets, mixed together with graphene oxide. In $Ti_3C_2T_x$ nanosheet, terminal T_x = F, −O, and −OH.

They have successfully demonstrated that the addition of MXene filler into chemically modified Graphene foam materials allows improving not only their THz absorption that is of up to 4.6×10^4 dB cm^3 g^{-1}, but also their mechanical stability under compressive strain (50%) of at least 200 cycles. On top of that, the heating step in the process and its associated cost were eliminated.

In all these approaches, material composites are made up of an extra carbon phase consisting mainly of sp^2 hybridized carbon, which is added and dispersed into a polymeric matrix or any other mixtures.

It is only recently, our research group suggested another way of considering the polymeric matrices and to think of them as potential precursors of sp^2 carbon phase needed for THz absorption.

2.5 | Polymer-derived carbons

For the first time, as an alternative to sp^2-Carbon of graphite and composites, disordered sp^2 carbon materials issued from thermal conversion of polymers was suggested and investigated by Hourlier's team.[40,52–55]

The main advantage of such disordered carbonaceous materials is that their physical properties can be varied according to the heat treatment temperature, treatment atmosphere, molecular architecture, and cross-linking state of polymers. For example, pyrolysis of cellulose ($C_2H_{12}O_6$) yields a disordered carbon that has variable properties depending on the temperature of heat treatment. The electrical conductivity of cellulose varies from 10^{-10} to 1 S cm^{-1} when the treatment temperature increases from 400°C to 1100°C.[56] At the same time, the thermal conductivity of cellulose also changes from 0.1 to 0.8 W m^{-1} K^{-1}.[57] Such disordered carbon consists of a turbostratic structure, which corresponds to an arrangement of graphene layers disoriented to each other, as shown in Figure 5B. Transmission electron microscopy (TEM) studies of carbonaceous materials, resulting from pyrolysis of various precursors such as coal-tar pitches, petroleum fractions, anthracene, and saccharose, reveal the presence of building blocks, the so-called basic structural units (BSU).[24] The BSU are a stack of two or three graphene layers, with a total diameter of ~1 nanometer.[24] The disordered carbon can be characterized by two parameters, namely the crystallite size or coherence length along the a-axis (L_a) and c-axis (L_c). Figure 8 illustrates the various steps involved in the preparation of carbon-based materials.

In short, the fabrication of materials containing carbon is obtained via a chemistry-route that involves three main steps: synthesis of monomers, followed by a subsequent cross-linking step using appropriate functional groups that allow the formation of branched products. Generally, the cross-linking occurs at moderate temperatures. This step is necessary and brings about high yields during the subsequent thermal treatment. The third and final step is pyrolysis. The term pyrolysis is commonly used by ceramists to refer to the thermal process wherein the sample undergoes chemical modifications in an inert or reductive environment. In the case of pyrolysis of organic polymers, the final residue is a solid carbonaceous material (either coke or char), whereas hybrid organic–inorganic polymers are thermally converted into ceramic residue containing free carbon phase.[25] In order to obtain crystalline materials, the residues are subjected to heat-treatment at high temperatures (1500°C–3200°C). The heat treatment of coke gives graphite, whereas char results in vitreous carbon. For any potential application, the selection criteria of the polymeric precursors are the following:

- High residue yield, which is defined as percentage mass of the solid residue remaining at the end of pyrolysis process;
- Easy to process into various shapes, and net-shaped after thermal conversion.

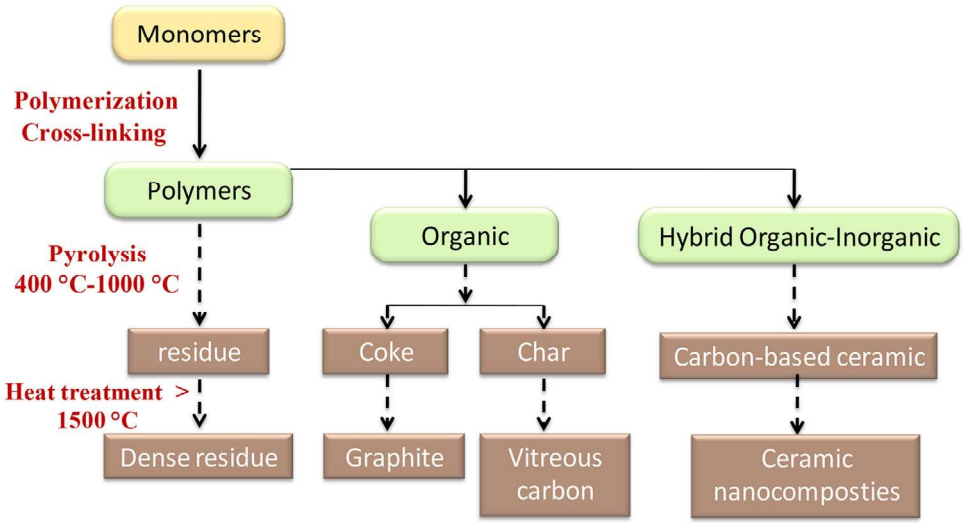

FIGURE 8 Processes involved in polymer-derived materials

Two kinds of polymer, namely organic polymer (polyimide Kapton) and hybrid organic-inorganic polymer (polydimethylsiloxane, PDMS) were investigated.

Polyimide film undergoes physical and chemical changes when heat-treated in an inert atmosphere. During the course of pyrolysis of the polyimide, a large weight loss (40 wt.%) occurs between 400°C and 800°C, due to the breaking of polymer chemical bonds. Thermal degradation leaves a solid carbonaceous residue and generates a variety of volatile species consisting principally of H_2, H_2O, CO, CO_2, HCN, and also relatively higher molecular weight species, such as benzene and its derivatives. As in most organic polymers, polyimide degradation ultimately results in decreased flexibility, with shrinkage of around 20%, and in a discoloration from transparent amber to visibly opaque black material. The solid carbonaceous residues exhibit electrical conduction characteristics as well. D.C. electrical conductivity increases from 0.23×10^{-3} to 298 S cm^{-1} as the heat treatment temperature rises from 700°C to 1200°C. The thickness of the material, as well as its free-carbon content and its structural rearrangement can cause significant deviations in how a sub-millimetric wave is transmitted, and reflected, leading to different rates of absorptions. The maximal absorption of 47% was obtained with the Kapton HN annealed between 750°C and 800°C. This result corroborates the model developed by Hadley–Dennison for a single layer of metal that can absorb a maximum of 50%.[40] For this reason, as with metals, the use of Kapton-derived carbon as absorber in thermal detector applications is limited. However, this is not true in EMI shielding applications, for which the desired shielding effectiveness of Kapton-derived carbons can be tailored by controlling the process parameters of the heat treatment (see Figure 6). The paramount advantage of Kapton-derived carbon is that the total elimination of the complexity involved in mechanical mixing of two distinct phases to make a composite.

The starting polymer PDMS, offers the advantage that it can into complex shapes and with a large surface area, while also being easy thermally converted into ceramic materials.[53] Hydrocarbon groups bonded to silicon atoms ($Si\text{-}CH_3$) are a source of condensed phase free carbon needed for THz absorption. The soft and flexible PDMS cross-linked polymer has a refractive index of 1.55 and a high absorption coefficient of 15 cm^{-1} in the frequency domain 500–750 GHz. Different process variables, such as pyrolysis temperature, or texturing surfaces can induce changes in the physical properties of resultant materials.[52] By varying the pyrolysis temperature between 450°C and 1500°C, the absorption coefficient changes from 5 cm^{-1} to 46 cm^{-1}, and the refractive index from 1.58 to 2.05. In the material chart below (Figure 9), the refractive index and absorption coefficient of various materials are compared.

The starting polymers have a small refractive index ($n_{Kapton} \sim 1.88$, $n_{PDMS} \sim 1.55$) and low absorption coefficients ($\alpha_{Kapton} \sim 12\ cm^{-1}$, $\alpha_{PDMS} \sim 15\ cm^{-1}$). These values progressively increase and displace towards the domain of C sp^2 (graphite, CNTs) as the heat treatment temperature increases. The transition from polymer to sp^2 carbon-based materials is clearly seen in Figure 9.

Heat-treated carbonaceous materials with different transmission and reflection characteristics can be accurately reproduced by controlling pyrolysis parameters (temperature, duration, and atmosphere). The advantage of the thermal conversion of organosilicone polymers, when compared with conventional mixing or melting

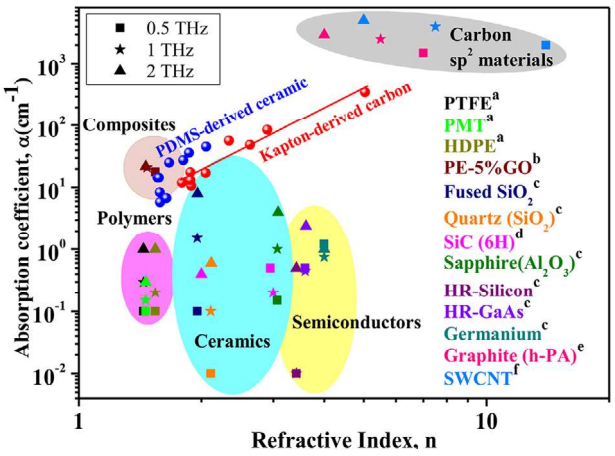

FIGURE 9 Optical constants of most commonly used materials at 0.5 THz (squares), 1 THz (Stars), and 2 THz (triangles); a – Brundermann et al.,[2] b – Pedro et al.,[34] c – Grischkowsky et al.,[58] d – Strait et al.,[59] e – Gusakov et al.,[22] f – Maeng et al..[60] Kapton-derived carbon (in red)[40] and PDMS-derived ceramics (in blue)[52]

processes, lies in the much greater control over the content and distribution of free carbon phase in the oxide system. For absorbing terahertz frequencies, the presence of sp^2 carbon is necessary but not sufficient in and of itself. Carbon must be at least partially organized into a few stacked-graphene layers, whatever their orientation.

For PDMS-derived ceramics obtained at 1500°C, a reflectivity of –3 dB was obtained for planar surfaces, whereas pyramidal surfaces exhibited a much lower value of –22 dB when measured at oblique incidence and a receiving angle of 60°.[52] The flat sample heat-treated at 1500°C shows absorbance of 78% over the broadband 0.2 to 3 THz.

3 | APPLICATIONS OF TERAHERTZ ABSORBERS

Efficient absorption of THz radiations has been exploited in a wide range of devices as shown in Figure 10. THz absorbers can be classifed based on their spectral response: broadband and narrowband absorbers. Broadband absorbers are analogical to low-pass filters, which means that reflection is minimized above the cut-off frequency leading to total absorption.[2] The narrowband absorbers are analogical to band pass filters, where the pass/stop frequency can be varied by adjusting the geometry and periodicity of the resonating structures.[61–63]

3.1 | Thermal source

THz sources are the key elements for the most promising applications such as spectroscopy, imaging devices and telecommunications. Several approaches are available to generate THz radiation, namely, Schottky diode harmonic generation,[64] quantum cascade laser,[65] molecular laser emission,[66] thermal sources (blackbody radiators) and also transistor-based technologies.[67] The natural source of THz radiations is the Sun and the cosmic background, but they are available only in space as the moisture in the Earth's atmosphere strongly absorbs the incoming THz radiations. The common thermal source used for laboratory purposes are a mercury lamp,[68] and a Globar plug - silicon carbide (SiC) electrical heater.[69]

A blackbody source operating at high temperatures 1200°C–1380°C delivers emissivity in the range from 0.5 to 0.8 (no units),[69] and generates power of a few μW.[70] One of the drawbacks of such a thermal source is the emitted wavelengths which cover not only THz but also mid-infrared and visible wavelengths. Selective filtering of the unwanted radiations while transmitting the desired THz radiation is a challenging task.[70] Planck's radiation law states that the maximal power density of the emitted radiation at wavelength (λ) depends on the temperature of the blackbody. Svetlitza et al.[70] calculated the ratio between the power density of "wanted" THz radiation and the maximal power density of the radiation emitted at various temperatures. The ratio decreased down to 4 $\times 10^{-6}$ as the blackbody temperature increased to 1227°C (1500 K). In otherwords, for a thermal source operating at high temperatures, filters with very high attenuation are required to prevent the unwanted IR radiation while transmitting the THz radiation.[70]

The characteristics of material required for a good thermal source are: a perfect absorber for the maximum emission; materials operating in ambient conditions without need of vacuum tubes; and materials that can filter unwanted mid-IR radiation and also have good chemical stability at low and high temperatures even after a long service life. Recently, the high emissivity of carbon

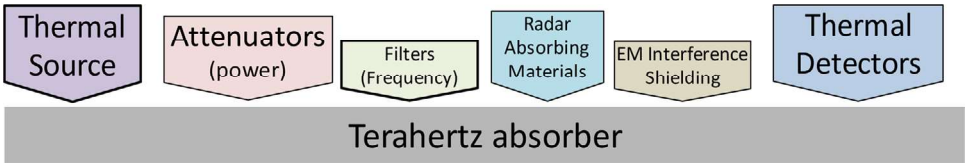

FIGURE 10 Various applications that rely on the material's efficient absorption of terahertz radiation properties

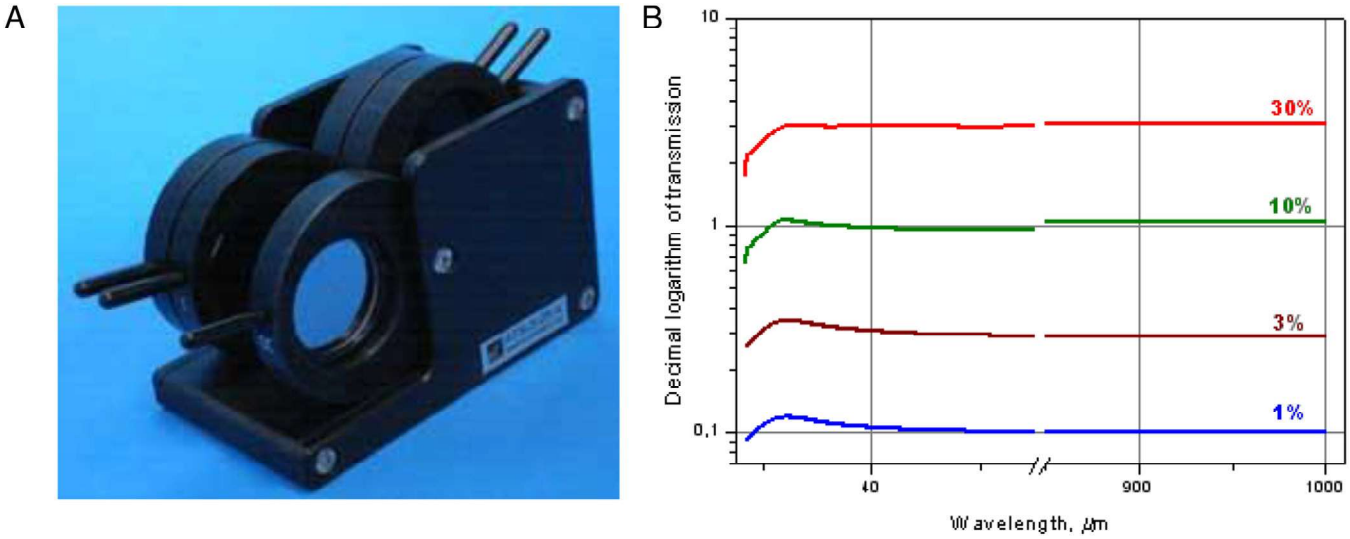

FIGURE 11 Silicon-based variable wheel attenuators (source: Tydex website[74])

has been exploited for use as THz radiation source. Thus, Carbon nanotube (CNT), fiber bundles of diameter 10–15 μm enclosed in N_2 gas bulb, resulted in a shorter and more intense pulses of terahertz radiation than conventional metal-alloy emitters.[71] Actually, Dong et al.[73] theoretically predicted that THz emission of the order of a few ~mW cm^{-2} is possible from a suspended graphene supplied with D.C. electrical field.

3.2 | Attenuators

Power attenuators are used in device testing laboratories, particularly in spectrometers. Materials with terahertz absorbance independent of frequency are usually preferred. As shown in Figure 11, the commercially available attenuator is based on silicon wafers (Tydex, Russia[71]). The attenuator wheels made of silicon wafers can be arranged in a consecutive manner to attain discrete levels of attenuation 30%, 10%, 3%, and 1%. By combining the wheels, attenuation even down to 0.0009% can be achieved.[71] However, such a configuration produces a standing wave and causes strong back reflection (~30% at normal incidence for Si) that can therefore induce perturbations to the emitter. Various options to overcome these problems have been proposed, which include

(i) tapering the wafers, so that the reflected radiation is redirected away from the area of measurement,
(ii) anti-reflection coatings of thickness $L_s = \lambda/4$, and of refractive index $n_{coating} = \sqrt{n_{substrate}}$ which can create destructive interference. For example, polyimide ($n = 1.88$) with a thickness of 125 μm coating can be used on silicon substrate ($n = 3.5$) to avoid reflection at 0.6 THz.

Low-refractive index polymers are one of the low-cost alternatives to the silicon-based attenuators. Teflon or Polyethylene can be used as terahertz attenuators in the form of sheets or discs. However, attenuating the incident beam to lower power levels may require thicker materials.

Iida et al.[72] fabricated attenuators based on metallic films. Various thicknesses of Inconel alloy were sputter deposited on thin polyester films to achieve attenuations of −3 dB, −6 dB and −12 dB. Transmittance down to −24 dB was achieved by stacking attenuators via a programmable system. The authors developed a calibration curve that was further sucessfully implemented to quantify the unknown concentration of maltose embedded in polyethylene matrix.[72]

For attenuators, the composite materials are a straightforward solution as the THz attenuation can be controlled by the filler, (size, content, structure and morphology) as already discussed in the Section 2.2. As a reminder, the polymer matrix composite materials with carbon-based fillers show gradual decrease of transmission with increasing filler content. Among various carbon-based materials, the newly developed attenuators based on heat treated organic polymer, Kapton, is a promising material to perform an accurate calibration of terahertz attenuation.[40]

3.3 | Filters

THz filters are used to eliminate any unwanted shorter-wavelength (infrared) radiations. The filtering can be performed in various ways[75] namely, selective absorption,

selective reflection or interference.[76] In selective absorption filters, the filtering relies on the intrinsic property of materials.[77] In that case, the materials can be readily used in their bulk form without any preparation. One of the advantages of absorption-type filters is that the angle of misalignment of the filter is up to ± 10° perpendicular to the incident beam, whereas reflection-type filters require a perfectly perpendicular position of the filter to the incident beam. Good examples of absorption filters are black polyethylene,[2] several alkali Halides (BeO+ZnO, TiCl+TiI+NaF, Cr_2O_3+Al_2O_3+PbF_2, CaF_2+LiF).[2] Another type of filter is the so-called metamaterials. It consists of a periodic array of metal/dielectric geometrical structures fabricated via complex lithographic techniques.[61] The metamaterials are preferred only for narrow-band filtering.

In telecommunication systems, the filters can also be used to modulate the signal. Among carbon-based materials, Carbon Nanotubes and Graphene gain attention, as they are compatible with the existing semiconductor technology and have been exploited for tunable filtering and modulation in the terahertz band, as described in a recent review.[78]

3.4 | Radar absorbing materials (RAM)

Radio detection and ranging (Radar) is defined as a device that transmits an EM wave and detects objects by virtue of the energy scattered from them in the direction of the receiver.[79] The devices operate at frequencies ranging from 3 MHz to 1 THz or higher. In military applications, an aircraft/ship is hidden from the radar device of enemy by absorbing all the incident radiations. For such purposes, absorbing materials with the following criteria are required[80]

- low reflectance (−30 to −40 dB) over the frequency range of operation, and at all angles of incidence
- stable materials in harsh atmospheres, without degassing any dust/vapors
- light-weight materials

For the millimetric wavelength domain ranging from 30 GHz to 300 GHz, the used materials[81] are metal (aluminum, iron oxide, nickel chromium alloys), conducting polymers (partially oxidized polypyrrole, Latex), carbon-based materials, and their composites. For an absorber, the low refractive index associated with high absorption coefficient are necessary characteristics, but not sufficient. The geometrical configuration of the absorber plays a major role in the efficient absorption of the incident radiations. For example, a pyramidal absober is a well-known

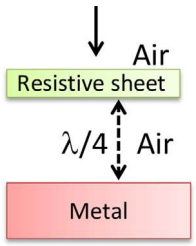

FIGURE 12 a schematic diagram of the Salisbury screen

efficient geometrical design. The height and periodicity of the pyramids are about the same size as the wavelength. The pyramidal structure increases the probability associated with multiple interactions of the radiation through material. Jussi et al.[80] compared the performance of commerically available pyramidal absorbers such as TK THz RAM (Thomas Keating Inc, UK), FIRAM-500 and TERASORB-500 (Umass Lowell, USA). The TK THz RAM was found to have the lowest specular reflectivity down to −50 or −40 dB. It is made of carbon-loaded polypropylene plastics, and the pyramidal shape is obtained by injection molding technique.[80] The TK THz RAM has the following dimensions: pyramidal heights of 1.5 mm, spacing of 1.0 mm and opening angle of 33.7°.[80]

Another example is the Salisbury screen, in which a resistive sheet (e.g., thin carbon or metal coating) is separated at a distance of odd multiple of ij wavelengths from a metal plate (Figure 12). The separated region could be air or low-loss dielectric. For example, 9 nm thin film of Inconel on Mylar, and 250 μm thick polystyrene foam spacer has reflectance = −22 dB at 0.88 THz.[82]

Recently, Woo et al.[83] demonstrated a Graphene-based Salisbury screen in which single-layer Graphene was chosen as the resistive layer, Zeonor (Cyclo-olefin polymers,98 μm thick) as a low-loss dielectric, and Gold thin film (200 nm) as the reflector. For maximum absorption, the sheet resistance of single-layer graphene was expected to be equal to the free-space (377 Ω $\square^{-1}$) as predicted by simulations. Achieving the desired sheet resistance through doping seems difficult. They designed graphene samples of three different sheet resistances 1295 ± 10 Ω $\square^{-1}$ (undoped), 817±20 Ω $\square^{-1}$ (66 wt.% HNO_3, p-type, doping time, 2 min) and 689 ± 5 Ω $\square^{-1}$ (doping time, 3 min). The Salisbury screen fabricated with 689 Ω $\square^{-1}$ exhibited the maximum absorption of 0.95 and 0.97 at 0.5 THz and 1.5 THz, respectively. Wu et al.[84] fabricated a five-layer stack of graphene on quartz substrates by the layer-by-layer transfer process. The authors demonstrated that increasing the number of graphene layers resulted in decrease of transmission from 90% to 83% in the visible domain, whereas in the 0.125 THz–0.165 THz frequency range, a strong standing wave (Fabry–Perot) is generated between

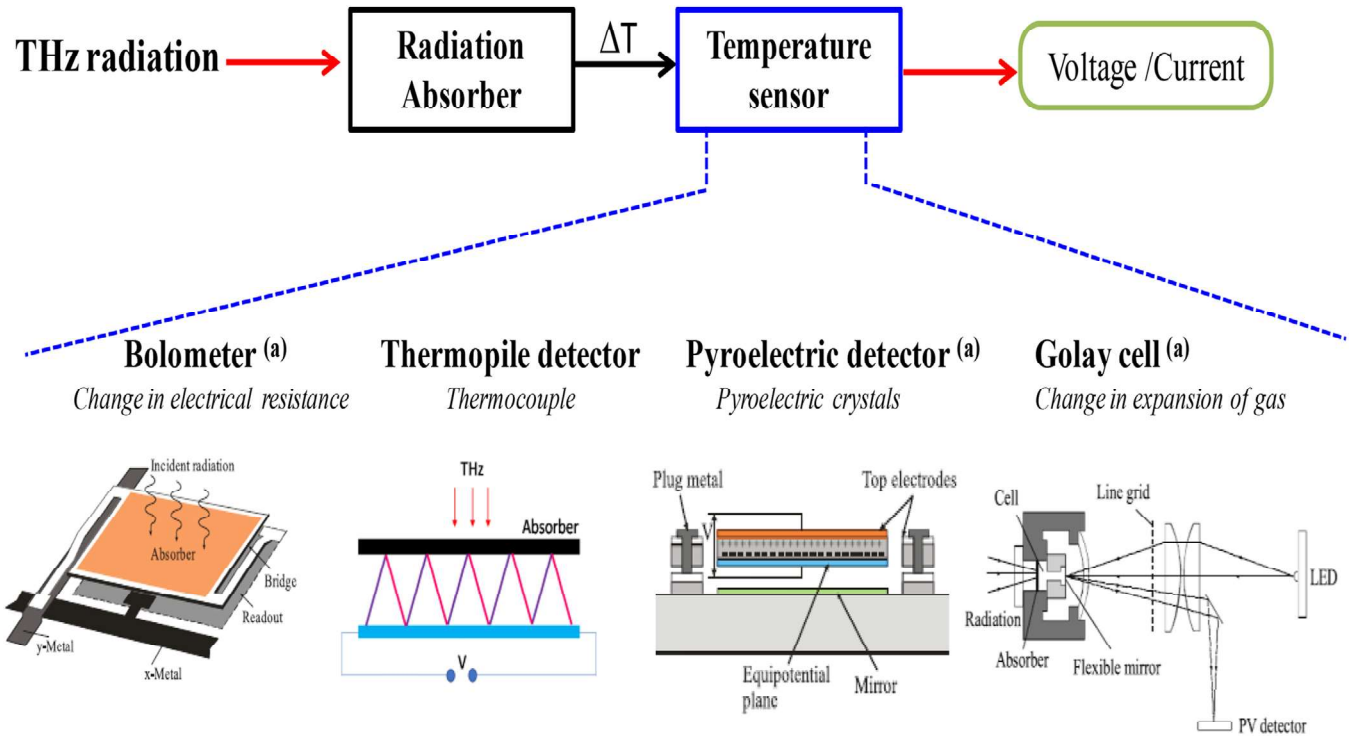

FIGURE 13 Thermal detectors used for THz frequencies; a – Rogalski et al[85]

the graphene and the quartz, resulting in the absorption of 90% over a bandwidth of 28% for the 4-layers of graphene on quartz. Despite its popularity, graphene that is used for devices fabrication has some drawbacks related with fabrication of large-area, and a tight control over the sheet resistance of the graphene.

3.5 | Thermal detectors

In thermal detectors, the THz radiation is detected by measuring the heat energy produced in the material due to the absorption of incident radiation. In other words, a thermal detector consists of a "radiation absorber" and a "temperature sensor". The absorber converts the incident THz radiation into heat, and the subsequent temperature variation is detected by the temperature sensor that delivers either voltage or current corresponding to the incident radiation. The thermal detectors should be able to measure the broad spectral domain due to the fact that the thermal effects depend only on the absorbed radiation power but not on the photon energy. The thermal detectors can be classified according to the physical principle used to measure temperature (Figure 13). For example, bolometers utilize the change in electrical resistance, whereas Golay cell records the change in the thermal expansion of gas.

There are many different tools for measuring temperature:

- Thermocouples, that is, two dissimilar metals are joined together to form two junctions. A voltage is delivered in the circuit when one side of the junction is hot and the other side is cold. Many thermocouples are connected in series or in parallel to form a thermopile, so that incident THz radiations induce heat at the junction of thermopiles (Figure 13). The materials used for thermopile detectors are Ti-Al, Bi-Cr, Ti-doped Si and Si-Ge.
- Pyroelectric crystals generate positive and negative charges on the two opposite surfaces of the crystal due to heating. In pyroelectric detectors, (Figure 13), an absorber layer is deposited on the pyroelectric crystals. The materials used as pyroelectric crystals are Lead zirconate titanate (PZT), Barium strontium titanate (BST), Triglycine sulfate (TGS) and Polyvinylidene difluoride (PVDF).

3.6 | Detector parameters

The performance of the thermal detector depends on many factors such as THz absorbance, the heat capacity of the absorber, the accuracy of the temperature rise measured and the thermal conductance between the heat source and heat sink. Besides the physical properties of materials used in the device, the geometrical design also influence the performance. The performance of a thermal detector is evaluated on the basis of the following criteria:

- Higher the responsivity of the thermal detector, sensitive the device is. Responsivitiy ($\Re$) is a ratio of measured voltage (or current) to the incident power. It is expressed in Volts per Watt (V/W). At the visible and near infrared range, most thermal detectors have spectrally flat responsivity, whereas below 1 THz (> 300 μm) the responsivity is low, as the photon is not being absorbed.
- The lower the NEP value is, the better the sensitivity of the detector. Noise-equivalent power (NEP) is the common metric that quantifies a thermal detector's sensitivity or the power generated by a noise source. Rogalski et al.[85] define NEP as follows: the value of root mean square (rms) of incident power on the detector generating a signal output equal to the rms noise output. Several factors may contribute to the total noise of a thermal detector. For example, the current passed through a resistor generate thermal agitation, the so-called Johnson noise. The voltage genetrated by Johnson noise is $V_n = \sqrt{4\,\kappa_b T_a\, R_{d.c.}\, B}$, where $R_{d.c.}$ is the electrical resistance (Ohm) of the resistor, T_a is the temperature in Kelvin, k_b is the Boltzmann constant (1.38×10^{-23} m^2 kg s^{-2} K^{-1}) and B is bandwidth of the measurement (typically, 1 Hz). The NEP (W Hz$^{-1/2}$) is ratio of Johnson noise voltage (V_n) to responsivity ($\Re$). The NEP is in the range of 10^{-13} to 10^{-6} W Hz$^{-1/2}$.
- A shorter 'τ' is desirable for rapid disspiation of heat, and thus suitable for use of the detector as a thermal camera. The time constant (τ) expresses the speed at which a device responds to a change in incident power. Bründermann et al.[2] define the time constant as follows: "It is the time required for the output signal of a detector to rise 63.2% of its final value, when it is abruptly exposed to a continuous field of electromagnetic radiation". The time constant of a thermal detector depends on the heat capacity of the absorber and thermal dissipation configuration of the device. The time constant ranges from few milliseconds to seconds.
- Specific detectivity D^* must be as large as possible. Specific detectivity (D^*) is a parameter that accounts for the sensitive area of the device. It is the ratio of the square root of the area ($\sqrt{A}$) to NEP, expressed in cm$\sqrt{\text{Hz}}$ W^{-1}. For thermal detectors, specific detectivity varies from 10^7 to 10^{10} cm$\sqrt{\text{Hz}}$ W^{-1}.

3.7 | Comparison of thermal detectors

Table 2 shows the comparison of the most used THz thermal detectors, operating at room temperature.

Among various commercially-available thermal detectors that operate at room temperature, the Golay cell has the highest sensitivity (NEP = 0.14×10^{-9} W Hz$^{-1/2}$, $D^* = 7.59 \times 10^9$ cm$\sqrt{\text{Hz}}$ W^{-1}), but it is very sensitive to mechanical vibrations, and requires an external power supply to run. Moreover, the membrane used in the Golay cell is fragile. The largest area (> 50 mm) device is the calorimeter (Scientec, USA) and their performance below 8 THz has not been reported. The vertically-aligned carbon-nanotubes (VANTA) absorber showed maximum absorption of 99% at 0.76 THz.[86] It was found that the reflectivity of the absorber varies with the length of the CNTs. A minimum reflectance was obtained for CNTs of 1.5 mm length at 0.75 THz.

Absorption at frequencies lower than 0.75 THz has not been reported. The Pyroelectric detector (Gentec-EO, Canada) consists of a volume-absorber that has a maximum absorption of 80% over broadband (0.1 to 30 THz). Although devices with different area can be found, the detector has the slowest time response (time constant 3 seconds). To increase the absorption further, Muller et al.[16] used three identical detectors arranged at an angle of 45° to each other, As shown in Figure 14, the incoming radiations interact at least five times before completely absorbed, that is, the total absorbance is $A = 1\text{-}R^5$ the summation of all three detectors reached 97% over the entire THz domain.

The highly sensitive commerical hot-electron bolometer (QMC Instruments Ltd., UK) operates at liquid-helium temperature 4.2 K. It uses a InSb semiconductor mounted on quartz substrate. The maximum sensitivity (NEP = 5×10^{-13} W Hz$^{-1/2}$, time constant = 300 ns) is achieved only if it is cooled to a few Kelvin (4.2 K) using liquid Helium or even to 1.5 K by reducing the vapour pressure above the Helium-4 reservoir.[87] The currently available metrological standard detector (PTB, Germany) consists of Schott AG's optical neutral density glass (NG1 glass), attached to a thermopile temperature sensor (3A-P, Ophir Optronics Ltd.). The NG1 glass has an optically polished surface, a thickness of 0.6 mm and a coating gold on the back. The purpose of the gold coating is reflecting the radiations back to the NG1, particularly for those having frequencies below 1 THz. The reflected radiations undergo several back and forth reflections (inset of Figure 15A) as the surfaces of the glass are flat. The transmittance and reflectance spectra of the NG1/Gold sample of 0.57 mm is shown in Figure 15.

The NG1 glass/gold is partially transparent at frequencies lower than 0.6 THz, the sinusoidal pattern corresponds to the standing wave occurred inside the NG1 glass. On the other hand, the reflectance varies between 18% and 10% in the frequency range 1 THz to 5 THz.

The calibration of the standard detector is performed in the visible domain (He-Ne laser), where the maximum absorbance is attained, and then a numerical factor is

TABLE 2 Comparison of terahertz thermal detectors operating at 300K

Area ϕ dia [mm]	Absorbance [%]	NEP [W $Hz^{-1/2}$]	Time constant [ms]	Specific detectivity D* [cm$\sqrt{Hz}$ W^{-1}]	Remarks
Calorimeter (Scientech Inc., USA), Volume absorber, 8–1200 THz					Not suitable for frequencies < 8 THz
50.8	NA	10×10^{-6}	3	NA	
Pyroelectric (SLT, Germany), Metal/PVDF/Metal, 0.6–6 THz					50% absorbance, PVDF degradable over time
10	50	10×10^{-6}	50	8.86×10^{4}	
Photo-acoustic detector using closed air cell (Thomas Keating, UK),0.03 - > 3 THz					Thick optical window
30	50	5×10^{-6}	NA	5.32×10^{5}	
Pyroelectric (Gentec-EO, Canada), Organic Black layer (THz9D-20mS-BL) 0.1–30 THz					Organic black layer absorption is only 10% (0.5–1 THz)
9	10 (0.5–1 THz) > 60 (>3THz)	0.3×10^{-6}	200	2.66×10^{6}	
Pyroelectric (Gentec-EO, Canada), Volume absorber (THz9D-3S-VP) 0.1–30 THz					Highest absorbance, Slowest response
12	80	0.5×10^{-6}	3×10^{3}	2.13×10^{6}	
Golay cell (Tydex, Russia), 0.04–15 THz					High sensitivity, fragile, sensitivity to vibration, requires external power supply,
6	NA	0.14×10^{-9}	30	7.59×10^{9}	
Thermopile pad and Pyroelectric [86] CNTs/Alumina paste/thermopile or $LiTaO_3$, 0.76 THz					absorption not reported below 0.76THz, slow response
2.5 × 3.5 mm	99 (CNTs, 1.5 mm)	50×10^{-6}	500	1.87×10^{4}	
Microbolometer with pyramidal absorber[52] Polysiloxane-derived carbon/Pt resistor, 2.5 THz					broadband absorption, high sensitivity, moderate response
0.4 × 0.42 mm	78	2×10^{-9}	80	26×10^{6}	
Minimum Value;	Maximum Value				
Here below, the characteristics of the high sensitivity hot-electron bolometer (4.2K) and the metrological standard detector has been given as additional information					
Hot-electron bolometer (QMCI, UK), InSb on Quartz, Winston cone, 0.06–0.5 THz					High sensitivity, very fast, requires cooling down to 4.2 K, heavy cryostat 15–40 kg
5 × 4.7 mm	NA	5×10^{-13} (at 4.2K)	3×10^{-4}	9.7×10^{11}	
Metrological Standard Detector (PTB, Germany), SCHOTT NG1/Au coating at back/Thermopile, 0.2 THz to visible					Poor absorption at lower frequencies, quantification of power is based on physical model
12	80–90 (> 1THz), 20–10 (0.2 0.7 THz)	NA	NA	NA	

NA, not available; Free-space (air): no antennas were used to couple the incoming THz radiations to the detector.

used to retrieve the responsivity at THz domain using the relation (6).

$$\text{Responsivity, } \Re(f) = \frac{\Re(HeNe)}{0.9562}\,[1 - \text{Reflectance}(f)] \quad (6)$$

where f is the frequency of incident radiation. This procedure uses a physical model to calculate the power responsivity, which is based on the reflectance. No information has been found regarding linearity at high power levels, and also on the thermal behavior of NG1 glass.

Recently, our research team has developed the first small polymer-derived absorber prototype. For the proof of concept demonstration, we have tested a broadband THz micro-bolometer using net-shaped pyramidal ceramic structures as absorbers.[52] A responsivity of 0.76 V/W, time constant of 180 ms, and noise equivalent power of

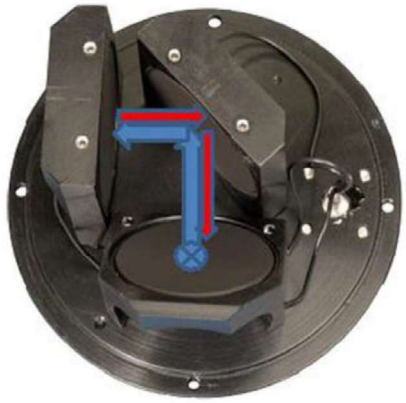

FIGURE 14 Commercial (Sensor-und Lasertechnik, Germany) pyroelectric THz detectors with trap design, adapted with permission from Ref[16]

$\sim$ 2 nW Hz-$^{1/2}$, have been achieved, thus putting it in fair competition with commercial thermal detectors.

Table 3 summarizes the advantages and disadvantages of commonly used materials for Terahertz wave's absorption for use in specific applications.

4 | CONCLUSION

Whatever the application is, the terahertz absorbing materials must have high absorption, and at the same time, low reflection. The available commercial absorbers, as a part of THz thermal detectors operating at room temperature, are particularly well suited in the two border frequency regions (microwave and infrared), but are not adapted to the THz domain.

The materials currently used as THz absorbers are either metal coatings or black composite materials consisting of two phases: a carbon-based phase (particles, nanotubes) dispersed into a polymeric matrix. Metals and carbon-based composites have shown some limitations in use. The major obstacle encountered for metals is their inherent high reflection of THz radiation, whereas for mixed-phase containing carbon composites, it is their low environmental stability due to their progressive degradation over time, partly as a result of their chemical composition and their complex manufacturing processes. However, the absorption performance of composites can be improved through a simplified manufacturing process, in which the step of mixing compounds is eliminated. The underlying advantage of avoiding the mixing step is to overcome the often encountered problems of distribution and dispersion of carbon-filler into a matrix.

To circumvent such obstacles, the most elegant and promising method to obtain a well-dispersed carbon phase, is the chemistry route via pyrolysis of polymers. Indeed, polymeric-derived materials have showed a greater ability to absorb THz radiation. Variable transmission and reflection characteristics of materials can be accurately reproduced by controlling pyrolysis parameters, and also by choosing appropriate functional substituent groups in the precursor. Moreover, polymer-derived materials are thermally stable at high temperatures, even in an oxidizing atmosphere for ceramics resulting from hybrid organic-inorganic precursors.

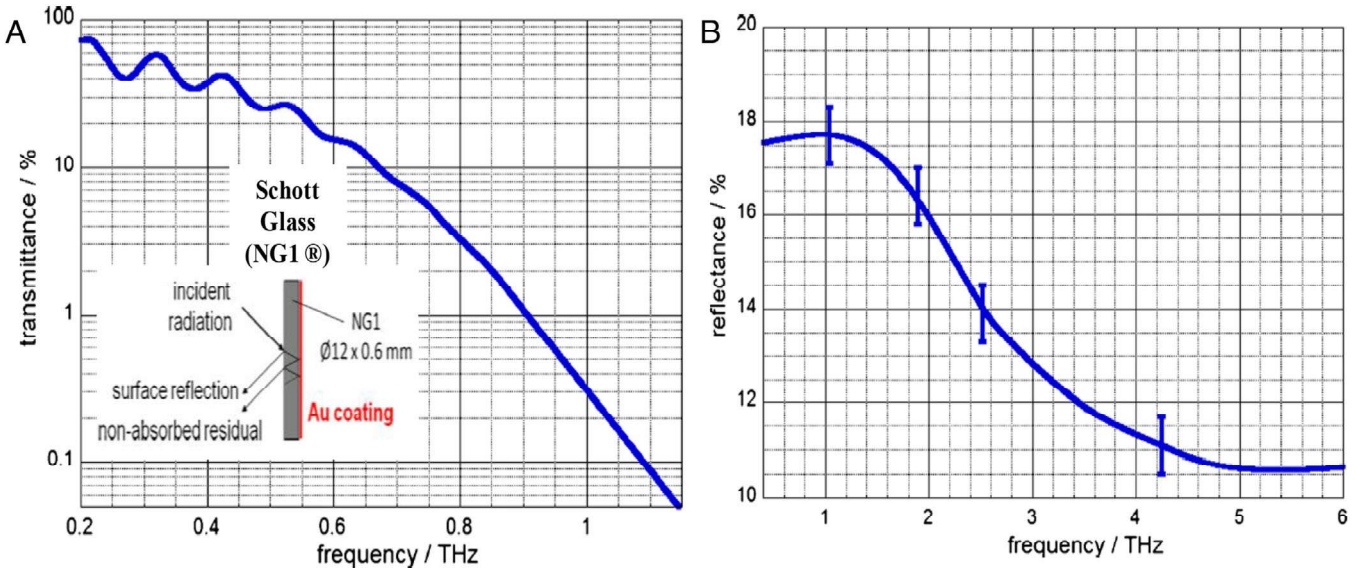

FIGURE 15 (A) transmission spectrum, (B) reflectance spectrum of NG1/Gold sample, thickness 0.57 mm. Adapted with permission from Ref[16]

TABLE 3 Most commonly used absorber materials for terahertz applications

Materials	Advantages	Drawbacks
Metals (Au, Ag, Cr, alloys)	Nanometric coatings Porous metal coatings (suitable for THz but not in IR)	Corrosive,Poor wettability,
Semiconductors (Si, Ge, GaAs)	Dopant/defect engineering Good thermal conductivity[b]	Parasitic reflection[a], Difficult to machine in mm scale
Carbon (Graphite, CNTs, Graphene)	The variety of allotropic forms, Good thermal conductivity[b]	Complex synthesis[b], reproducibility/ reliability, fragile
Dielectrics (Polymers)	Low cost, easy to shape	Thick (> 4 mm at 0.1 THz)[b,c] Molecular vibrational absorption[a]
Composites (Polymer matrix)	Magnetic particles or any other fillers can be incorporated as a second phase	Inhomogeneity, Reproducibility, Low thermo-oxidative stability[c]
Polymer-derived Materials	Near net-shaped structures, High thermo-oxidative stability	High thermal mass (heat capacity)[b]

[a] Attenuators.
[b] Thermal transducers.
[c] Radar absorbing materials.

It is to be expected that carbon-rich materials derived from the chemistry route of organosilicon polymers will find diverse applications and use, not only as absorbers in THz range, but also in the longer and shorter wavelength neighboring domains, that is, microwave and infrared. Another practical challenge is to find out whether this material could have a dual function, as absorber and as transducer, and would enable to convert the absorbed incident radiation energy into electrical energy.

ORCID

Djamila Hourlier https://orcid.org/0000-0002-4044-4429

REFERENCES

1. P. H. Siegel, Terahertz technology *IEEE Transactions on Microwave Theory and Techniques* **2002**, *50*, (3), 910. https://doi.org/10.1109/22.989974.
2. E. Brundermann, H. W. Hubers, M. F. G. Kimmitt, *Terahertz Techniques*, Springer, Berlin Heidelberg **2012**.
3. T. Nagatsuma, G. Ducournau, C. C. Renaud, Advances in terahertz communications accelerated by photonics *Nature Photonics* **2016**, *10*, (6), 371. https://doi.org/10.1038/nphoton.2016.65.
4. TeraHertz Full Body Screening | Tactical Solutions New Zealand, https://www.tactical.co.nz/terahertz-full-body-screening, accessed: May, 2020.
5. G. Terasense, Terahertz imaging Applications, https://terasense.com/applications/medical-diagnostics/.
6. M. Shur, Terahertz sensing technology, http://ieee-sensors.org/wp-content/uploads/2011/archive/Tutorials/THz_Sensor_Tutorial_10_26_08.pdf.
7. I. Teraview, Terahertz applications- Medical imaging, http://www.teraview.com/applications/medical/terahertz-medical-imaging.html.
8. P. U. Jepsen, D. G. Cooke, M. Koch, *Laser Photonics Rev.* **2010**, *5*, 124.
9. C. Yu, S. Fan, Y. Sun, E. Pickwell-MacPherson, *Quant. Imaging Med. Surg.* **2012**, *2*, 33.
10. W. R. Tribe, D. A. Newnham, P. F. Taday, and M. C. Kemp, "Hidden object detection: security applications of terahertz technology", Proc. SPIE 5354, Terahertz and Gigahertz Electronics and Photonics III, (8 April **2004**); https://doi.org/10.1117/12.543049.
11. P. Encrenaz, G. Beaudin, *Comptes Rendus Acadamie Sci. - Ser. IV - Phys.* **2000**, *1*, 1283.
12. G. Ducournau, F. Pavanello, A. Beck, L. Tohme, S. Blin, P. Nouvel, E. Peytavit, M. Zaknoune, P. Szriftgiser, J. F. Lampin, *Electron. Lett.* **2014**, *50*, 413.
13. G. Ducournau, Y. Yoshimizu, S. Hisatake, F. Pavanello, E. Peytavit, M. Zaknoune, T. Nagatsuma, J. F. Lampin, *Electron. Lett.* **2014**, *50*, 386.
14. C. Corsi, in THz Secur. Appl. (Eds: C. Corsi, F. Sizov), Springer Netherlands, Dordrecht **2014**, pp. 1–24.
15. S. Sankaran, K. Deshmukh, M. B. Ahamed, S. K. Khadheer Pasha, *Compos. Part Appl. Sci. Manuf.* **2018**, *114*, 49.
16. R. Müller, W. Bohmeyer, M. Kehrt, K. Lange, C. Monte, A. Steiger, *J. Infrared Millim. Terahertz Waves* **2014**, *35*, 659.
17. P. D. Cunningham, N. N. Valdes, F. A. Vallejo, L. M. Hayden, B. Polishak, X.-H. Zhou, J. Luo, A. K. Y. Jen, J. C. Williams, R. J. Twieg, *J. Appl. Phys.* **2011**, *109*, 043505(1.
18. M. A. Ordal, L. L. Long, R. J. Bell, S. E. Bell, R. R. Bell, R. W. Alexander, C. A. Ward, *Appl. Opt.* **1983**, *22*, 1099.
19. F. Alves, A. Karamitros, D. Grbovic, B. Kearney, G. Karunasiri, *Opt. Eng.* **2012**, *51*, 063801.
20. L. N. Hadley, D. M. Dennison, *J. Opt. Soc. Am.* **1947**, *37*, 451.
21. P. Delhaes, *Carbon Based Solids and Materials*, Wiley, New York **2011**.
22. P. E. Gusakov, A. V. Andrianov, A. N. Aleshin, S. Matsushita, K. Akagi, *Synth. Met.* **2012**, *162*, 1846.
23. M. N. Afsar, H. Chi, *Int. J. Infrared Millim. Waves* **1994**, *15*, 1161.
24. A. Oberlin, *Carbon* **1984**, *22*, 521.
25. M. Monthioux, O. Delverdier, *J. Eur. Ceram. Soc.* **1996**, *16*, 721.

26. T. D. Nguyen, S. Liu, G. Kumar, A. Nahata, Z. V. Vardeny, *Appl. Phys. Lett.* **2013**, *102*, 171107.
27. M. A. Seo, J. W. Lee, D. S. Kim, *J. Appl. Phys.* **2006**, *99*, 066103(1.
28. A. Das, C. M. Megaridis, L. Liu, T. Wang, A. Biswas, *Appl. Phys. Lett.* **2011**, *98*, 174101.
29. J. Macutkevic, D. Seliuta, G. Valusis, R. Adomavicius, A. Krotkus, P. Kuzhir, A. Paddubskaya, S. Maksimenko, V. Kuznetsov, I. Mazov, I. Simonova, *Diam. Relat. Mater.* **2012**, *25*, 13.
30. J. Macutkevic, D. Seliuta, G. Valusis, R. Adomavicius, P. Kuzhir, A. Paddubskaya, M. Shuba, S. Maksimenko, L. Coderoni, F. Micciulla, I. Sacco, S. Bellucci, *Chem. Phys.* **2012**, *404*, 129.
31. J. Macutkevic, R. Adomavicius, A. Krotkus, D. Seliuta, G. Valusis, S. Maksimenko, P. Kuzhir, K. Batrakov, V. Kuznetsov, S. Moseenkov, O. Shenderova, A. V. Okotrub, R. Langlet, P. Lambin, *Diam. Relat. Mater.* **2008**, *17*, 1608.
32. H. Yan, X. Li, B. Chandra, G. Tulevski, Y. Wu, M. Freitag, W. Zhu, P. Avouris, F. Xia, *Nat. Nano* **2012**, *7*, 330.
33. A. Das, T. M. Schutzius, C. M. Megaridis, S. Subhechha, T. Wang, L. Liu, *Appl. Phys. Lett.* **2012**, *101*, 243108.
34. P. Chamorro-Posada, J. Vazquez-Cabo, O. Rubinos-Lopez, J. Martin-Gil, S. Hernandez-Navarro, P. Martin-Ramos, F. M. Sanchez-Arevalo, A. V. Tamashausky, C. Merino-Sanchez, R. C. Dante, *Carbon* **2016**, *98*, 484.
35. B. Sensale-Rodriguez, R. Yan, M. M. Kelly, T. Fang, K. Tahy, W. S. Hwang, D. Jena, L. Liu, H. G. Xing, *Nat Commun* **2011**, *3*, 1.
36. H. Jung Taek, P. Doo Jae, M. Jin Young, C. Soo Bong, P. Jae Ku, R. Farbian, P. Ji-Yong, L. Soonil, A. Yeong Hwan, *Appl. Phys. Express* **2012**, *5*, 015102.
37. M. A. Seo, J. H. Yim, Y. H. Ahn, F. Rotermund, D. S. Kim, S. Lee, H. Lim, *Appl. Phys. Lett.* **2008**, *93*, 231905.
38. M. Zdrojek, J. Bomba, A. Łapińska, A. Dużyńska, K. Żerańska-Chudek, J. Suszek, L. Stobiński, A. Taube, M. Sypek, J. Judek, *Nanoscale* **2018**, *10*, 13426.
39. Z. Huang, H. Chen, S. Xu, L.Y. Chen, Y. Huang, Z. Ge, W. Ma, J. Liang, F. Fan, S. Chang, Y. Chen, *Adv. Opt. Mater.* **2018**, *6*, (23), 1801165. https://doi.org/10.1002/adom.201801165.
40. S. Venkatachalam, D. Bertin, G. Ducournau, J. F. Lampin, D. Hourlier, *Carbon* **2016**, *100*, 158.
41. D. Polley, A. Barman, R. K. Mitra, *Opt. Lett.* **2014**, *39*, 1541.
42. T.-I. Jeon, K.-J. Kim, C. Kang, I. H. Maeng, J.-H. Son, K. H. An, J. Y. Lee, Y. H. Lee, *J. Appl. Phys.* **2004**, *95*, 5736.
43. Y. Zhou, Y. E, Z. Ren, H. Fan, X. Xu, X. Zheng, D. Yuan Lei, W. Li, L. Wang, J. Bai, *J. Mater. Chem. C* **2015**, *3*, 2548.
44. D. Polley, K. Neeraj, A. Barman, R. K. Mitra, *J. Opt. Soc. Am. B* **2016**, *33*, 2430.
45. K. Arts, R. Vervuurt, A. Bhattacharya, J. Gómez Rivas, J.W. Oosterbeek, A.A. Bol, *J. Appl. Phys.* **2018**, *124*, (7), 073105. https://doi.org/10.1063/1.5044265.
46. I. H. Baek, K. J. Ahn, B. J. Kang, S. Bae, B. H. Hong, D.-I. Yeom, K. Lee, Y. U. Jeong, F. Rotermund, *Appl. Phys. Lett.* **2013**, *102*, 191109.
47. S. Dong, Q. Shi, W. Huang, L. Jiang, Y. Cai, *J. Mater. Sci. Mater. Electron.* **2018**, *29*, 17245.
48. W. Ma, H. Chen, S. Hou, Z. Huang, Y. Huang, S. Xu, F. Fan, Y. Chen, *ACS Appl. Mater. Interfaces* **2019**, *11*, 25369.
49. Z. Huang, H. Chen, Y. Huang, Z. Ge, Y. Zhou, Y. Yang, P. Xiao, J. Liang, T. Zhang, Q. Shi, G. Li, Y. Chen, *Adv. Funct. Mater.* **2018**, *28*, 1704363.
50. A. K. Singh, A. Shishkin, T. Koppel, N. Gupta, *Compos. Part B Eng.* **2018**, *149*, 188.
51. A. K. Singh, A. Shishkin, T. Koppel, N. Gupta, in *Matererials for Potential EMI Shielding Applications* (Eds: K. Joseph, R. Wilson, G. George), Elsevier Amsterdam **2020**, pp. 287–314.
52. S. Venkatachalam, G. Ducournau, J.-F. Lampin, D. Hourlier, *Mater. Des.* **2017**, *120*, 1.
53. S. Venkatachalam, D. Hourlier, *Ceram. Int.* **2019**, *45*, 6255.
54. S. Venkatachalam, S. Lenfant, M. Depriester, A. H. Sahraoui, D. Hourlier, *Ceram. Int.* **2019**, *45*, 21505.
55. S. Venkatachalam, *Polymer-Derived Carbon Materials for Terahertz Wave Absorption*, University Lille Science and Technologies, Lille **2017**.
56. J. Ozaki, Y. Nishiyama, *J. Appl. Phys.* **1989**, *65*, 2744.
57. Y.-R. Rhim, D. Zhang, M. Rooney, D. C. Nagle, D. H. Fairbrother, C. Herman, D. G. Drewry Iii, *Carbon* **2010**, *48*, 31.
58. D. Grischkowsky, S. Keiding, M. van Exter, C. Fattinger, *J. Opt. Soc. Am. B* **1990**, *7*, 2006.
59. J. H. Strait, P. A. George, J. Dawlaty, S. Shivaraman, M. Chandrashekhar, F. Rana, M. G. Spencer, *Appl. Phys. Lett.* **2009**, *95*, 051912.
60. I. Maeng, C. Kang, S. J. Oh, J.-H. Son, K. H. An, Y. H. Lee, *Appl. Phys. Lett.* **2007**, *90*, (5), 051914. https://doi.org/10.1063/1.2435338.
61. T. Hu, C. M. Bingham, D. Pilon, F. Kebin, A. C. Strikwerda, D. Shrekenhamer, W. J. Padilla, Z. Xin, R. D. Averitt, *J. Phys. Appl. Phys.* **2010**, *43*, 225102.
62. X.-Y. Peng, B. Wang, S. Lai, D. H. Zhang, J.-H. Teng, *Opt. Express* **2012**, *20*, (25), 27756. https://doi.org/10.1364/oe.20.027756.
63. X. Shen, Y. Yang, Y. Zang, J. Gu, J. Han, W. Zhang, T. Jun Cui, *Appl. Phys. Lett.* **2012**, *101*.
64. A. Maestrini, J. Ward, G. Chattopadhyay, E. Schlecht, I. Mehdi, *Frequenz* **2016**, *62*, 118.
65. S. Kumar, Q. Hu, J. L. Reno, *Appl. Phys. Lett.* **2009**, *94*, 131105.
66. A. Pagies, G. Ducournau, J.-F. Lampin, *APL Photonics* **2016**, *1*, (3), 031302. https://doi.org/10.1063/1.4945355.
67. W. R. Deal, X. B. Mei, V. Radisic, K. Leong, S. Sarkozy, B. Gorospe, J. Lee, P. H. Liu, W. Yoshida, J. Zhou, M. Lange, J. Uyeda, R. Lai, *IEEE Microw. Wirel. Compon. Lett.* **2010**, *20*, 289.
68. K. Charrada, G. Zissis, M. Aubes, *J. Phys. D: Appl. Phys.* **1996**, *29*, (9), 2432. https://doi.org/10.1088/0022-3727/29/9/030.
69. V. M. Zolotarev, R. K. Mamedov, A. N. Bekhterev, B. Z. Volchek, *J. Opt. Technol.* **2007**, *74*, (6), 378. https://doi.org/10.1364/jot.74.000378.
70. A. Svetlitza, M. Slavenko, T. Blank, I. Brouk, S. Stolyarova, Y. Nemirovsky, *IEEE Trans. Terahertz Sci. Technol.* **2014**, *4*, (3), 347. https://doi.org/10.1109/tthz.2014.2309003.
71. A. Zubair, X. Wang, O. Drachenko, D. E. Tsentalovich, M. Pasquali, J. Kono, J. Leotin, "Pulsed black-body emitter based on current-driven carbon nanotube fibers," 2017 42nd International Conference on Infrared, Millimeter, and Terahertz Waves (IRMMW-THz), Cancun, **2017**, pp. 1–2, https://doi.org/10.1109/IRMMW-THz.2017.8066970.
72. H. Iida, M. Kinoshita, Y. Shimada, H. Kuroda, K. Kitagishi, Y. Izutani, *IEEE Trans. Instrum. Meas.* **2013**, *62*, 1801.
73. H. M. Dong, W. Xu, F. M. Peeters, *Opt. Express* **2018**, *26*, 24621.
74. Tydex, http://www.tydexoptics.com/en/products/thz_optics/thz_attenuator/.
75. J. M. Lamarre, J. Charlier, *Adv. Space Res.* **1982**, *2*, 79.

76. W. Withayachumnankul, B. M. Fischer, D. Abbott, *Opt. Commun.* **2008**, *281*, 2374.
77. Peters A. R. Ade, G. Pisano, C. Tucker, S. Weaver, A review of metal mesh filters, Proc. SPIE 6275, Millimeter and Submillimeter Detectors and Instrumentation for Astronomy III, 62750U (16 June **2006**); https://doi.org/10.1117/12.673162.
78. Z. T. Ma, Z. X. Geng, Z. Y. Fan, J. Liu, H. D. Chen, *Research* **2019**, *2019*, 6482975.
79. E. F. Knott, J. F. Schaeffer, M. T. Tulley, *Radar Cross Section*, Second , SciTech Publishing, Inc., Raleigh, NC 27613 USA **2004**. https://books.google.fr/books/about/Radar_Cross_Section.html?id=j7hdXhgwws4C&redir_esc=y.
80. A. V. R. Jussi Säily Otamedia Oy, *Studies on Specular and Non-Specular Reflectivities of Radar Absorbing Materials (RAM) at Submillimeter Wavelengths*, Helsinki University of Technology, Helsinki **2003**. https://citeseerx.ist.psu.edu/viewdoc/download?doi=10.1.1.127.9673&rep=rep1&type=pdf
81. P. Saville, *Review of Radar Absorbing Materials*, DTIC Document **2005**.
82. A. J. Gatesman, A. Danylov, T. M. Goyette, J. C. Dickinson, R. H. Giles, W. Goodhue, J. Waldman, W. E. Nixon, W. Hoen, **2006**, pp. 62120E-62120E–12.
83. J. Min Woo, M.-S. Kim, H. Woong Kim, J.-H. Jang, *Appl. Phys. Lett.* **2014**, *104*, 081106.
84. B. Wu, H.M. Tuncer, M. Naeem, B. Yang, M.T. Cole, W.I. Milne, Y. Hao, *Sci. Rep.* **2015**, *4*, 4130. https://doi.org/10.1038/srep04130.
85. A. Rogalski, F. Sizov, *Opto-Electron. Rev.* **2011**, *19*, (3), https://doi.org/10.2478/s11772-011-0033-3.
86. J. H. Lehman, B. Lee, E. N. Grossman, *Appl. Opt.* **2011**, *50*, 4099.
87. U. QMC Instruments Inc, http://www.terahertz.co.uk/index.php?option=com_content&view=article&id=215&Itemid=594.

How to cite this article: Venkatachalam S, Zeranska-Chudek K, Zdrojek M, Hourlier D. Carbon-based terahertz absorbers: Materials, applications, and perspectives. *Nano Select*. 2020;1:471–490. https://doi.org/10.1002/nano.202000067